

# Characterization of the Demagnetization Field in Iron-Nickel Nanopowder and Spark Plasma Sintered Samples

T. Ashokkumar<sup>1</sup>, A. Rajadurai<sup>2</sup>, A.H. Abishini<sup>3</sup>, A.H. Anchani<sup>3</sup> and Subash C.B. Gopinath<sup>4,5</sup>

<sup>1</sup>Marthandam College of Engineering and Technology College Road, Kuttakuzhi, Veeyannoor Post, (Near Marthandam) Kanyakumari District-629 177, Tamil Nadu, India

<sup>2</sup>Madras Institute of Technology, Chromepet, Chennai 600044, Tamil Nadu, India
<sup>3</sup>St. Joseph's College of Engineering, Old Mahabalipuram Road, Chennai-600119, Tamil Nadu, India
<sup>4</sup>Faculty of Chemical Engineering & Technology, Universiti Malaysia Perlis (UniMAP), 02600 Arau, Perlis, Malaysia
<sup>5</sup>Institute of Nano Electronic Engineering, Universiti Malaysia Perlis (UniMAP), 01000 Kangar, Perlis, Malaysia
ntashoknt.1966@gmail.com

Available online at: www.isca.in, www.isca.me

Received 3<sup>rd</sup> November 2024, revised 7<sup>th</sup> April 2025, accepted 8<sup>th</sup> June 2025

#### Abstract

This study investigates the impact of alloying elements; spark plasma sintering, grain size, and particle size on the coercive field (Hc) in iron-nickel alloys. The findings reveal that, generally, an increase in nickel content leads to a reduction in Hc after 2 hours of milling. However, in these two-hour milled samples, a notable increase in Hc is observed compared to the initial values of iron and nickel powders. This Hc increase may be attributed to the weakened particle-to-particle interaction between iron and nickel. Changes in Hc are closely linked to variations in grain and particle size. Hc values decrease as the grain size diminishes, ranging from 250 nm to 75 nm. Remarkably, a high Hc value of 103 Oe is observed in the 75 wt.% Ni-Fe alloy after 100 hours of milling, indicating the formation of single-domain grains. A decrease in Hc is noted until a critical particle size is reached; beyond this point, Hc values remain relatively constant until reaching a second critical dimension, after which Hc increases with decreasing particle size. Additionally, the study reveals that the Hc values in spark plasma sintered samples are consistently lower than those in the powder samples.

Keywords: Saturation magnetization; Spark Plasma Sintering; Alloyed power; Coercive Field.

#### Introduction

Recent studies have employed various methods to investigate and manipulate the properties of iron-nickel (Fe-Ni) alloys. Notably, You et al. utilized a self-designed magnetron sputtering system to coat copper material onto La-Fe11.65Si1.35 alloyed powder<sup>1</sup>. In contrast, Shamba et al. synthesized LaFe11.6Si1.4 alloy in a polycrystalline form through spark plasma sintering and arc melting methods<sup>2</sup>. Research efforts have explored the characteristics of bulk alloys, with particular attention given to Ni-Fe alloys, as seen in the works of Qazi et al.<sup>3</sup>, Polychronis et al.<sup>4</sup> and Barakat et al.<sup>5</sup>.

The fabrication of smaller-sized particles has also garnered interest. Techniques such as heat spraying for producing Fe-Ni nanoparticles<sup>6</sup> and mechanical synthesis of iron and nickel solid solutions using high energy ball milling<sup>7</sup> have been investigated. Furthermore, Du and Ramanujan<sup>8</sup> demonstrated mechanical alloying of Fe-Ni based magnetic nanostructures, while Bui et al.<sup>9</sup> analyzed the nanocrystalline properties of iron powders synthesized through ball milling techniques. Recent work by Ashokkumar and colleagues<sup>10,11</sup> focused on the saturation magnetization and magnetic retardation analysis of iron-nickel ball-milled nanopowders and sintered samples, respectively, using the spark plasma sintering (SPS) method.

A pivotal aspect of this research pertains to the coercive field (Hc) in Fe-Ni alloys. Yelsukov et al. 12 examined the nanocrystalline state of α-Fe through ball milling, highlighting its impact on magnetic and structural properties, particularly the increase in the coercive field. Sedlacek<sup>13</sup> posited that in soft magnetic materials<sup>14</sup>, Hc may be influenced by lattice defects and residual stresses, especially when domain sizes are comparable to the thickness of the Bloch walls. Conversely, in hard magnetic materials, heterogeneous particles of a size similar to the thickness of the Bloch walls tend to hinder the displacement of these walls. Additionally, in polycrystalline materials, the mobility of Bloch walls is significantly dependent on grain size, which also governs the initial permeability and coercivity. Coarse-grained materials tend to exhibit higher initial permeability and lower Hc compared to fine-grained ones, as an increased initial permeability necessitates a stronger magnetic field for remagnetization.

In this context, Figure-1 illustrates a hysteresis loop showing coercivity, while Figure-2 presents the variation in coercive force (Hc) values for different Fe-Ni alloys. These disparities in Hc values may be attributed to differences in grain sizes within the same alloys.

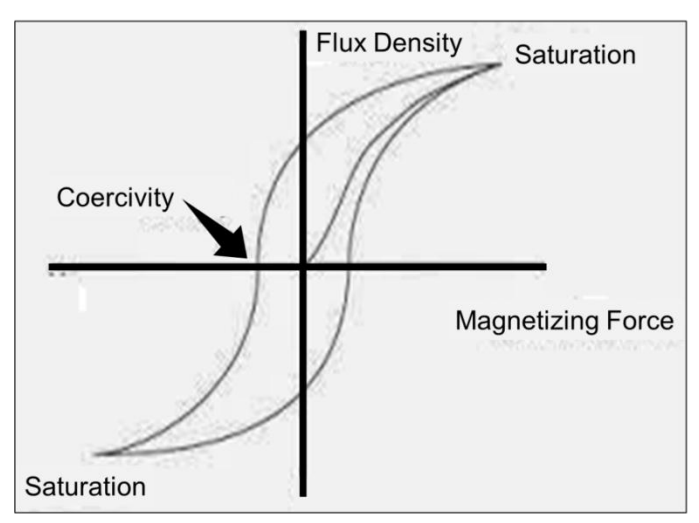


**Figure-1:** Hysteresis Loop Showing Coercivity.

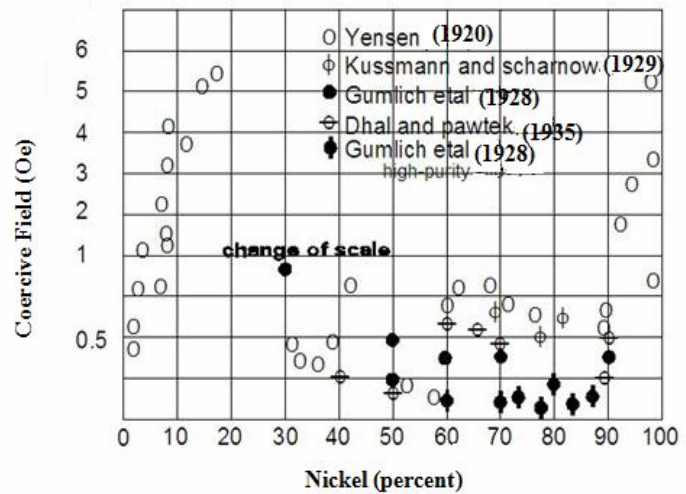


Figure-2: Coercive Force of Iron-Nickel Alloys<sup>18</sup>.

## Methodology

The purities of the initial nickel and iron materials were confirmed using energy dispersive X-ray (EDX) spectroscopy, which yielded purities of 99.8 wt% for nickel and 99.5 wt% for iron.

The procedures for powder preparation, blending, characterization, morphological observations, compositional analyses, and density determination have been previously detailed in Ashokkumar et al.<sup>14</sup>.

Magnetic properties of the starting nickel and iron powders, as well as the powders obtained after different durations of ball milling and the sintered specimens produced using Spark Plasma Sintering (SPS), were examined using a vibrating sample magnetometer (VSM). In the VSM, samples were centrally positioned within a uniform magnetic field and subjected to sinusoidal motion generated by mechanical

vibrations<sup>15</sup>. This motion induced changes in magnetic flux, resulting in a potential difference in the pick-up coils, directly proportional to the magnetic moment within the sample<sup>16</sup>.

Two thermal cycles, specifically at 923 K and 1223 K, were employed for the SPS process. Both thermal cycles utilized a compaction pressure of 30 MPa and a vacuum pressure of 6 Pa. Subsequently, small sections were excised from the sintered specimens and subjected to ultrasonic cleaning using acetone as the cleaning agent.

Prior to VSM analysis, the samples were accurately weighed using an electronic balance. The weighed powders were then folded in butter paper and placed within the VSM's powder sample holder. The magnetic field required to nullify the magnetization induced in the sample was deduced from the hysteresis loops generated with the assistance of the VSM.

## **Results and Discussions**

**Theoretical Density:** The theoretical density of powder mixtures, containing 40%, 50%, and 75% Ni-Fe, was determined by considering the densities of Fe and Ni, which are  $7.874 \times 10^3 \text{ kg/m}^3$  and  $8.908 \times 10^3 \text{ kg/m}^3$ , respectively.

**SEM Micrographs:** SEM micrographs provide valuable insights into the material's microstructure. Figure-3 displays an SEM micrograph of the 75% Ni-Fe sample after two hours of milling, offering a visual representation of the material's morphology at this stage.

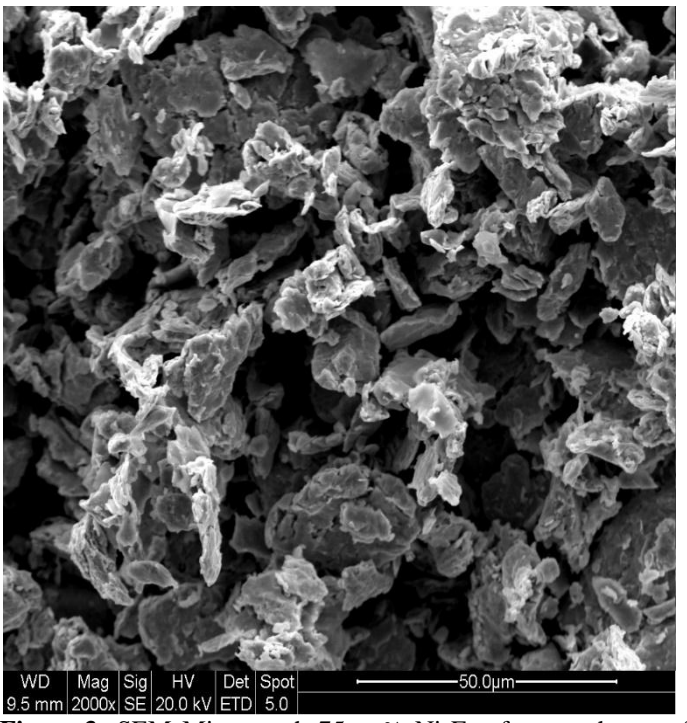


**Figure-3:** SEM Micrograph 75 wt% Ni-Fe after two hours of Milling.

**Magnetic Behavior:** Figure-4 presents the magnetic behavior of a 40% Ni-Fe powder sample after 16 hours of milling, as recorded by a vibrating sample magnetometer (VSM). This data is essential for understanding the magnetic properties of the material under various processing conditions.

XRD Diffraction Patterns: In Figure-5, we observe the X-ray diffraction (XRD) peaks of specimens sintered by spark plasma at different milling durations. The reduction in the width of XRD peaks with increased milling hours suggests enhanced grain growth in higher-hour milled spark plasma sintered samples. Moreover, spark plasma-sintered samples exhibit sharper XRD peaks compared to unsintered powders, indicating further grain growth during sintering.

Variation of Grain Size in Spark Plasma Sintered Specimens: Figure-6 depicts the relationship between grain size and milling hours in spark plasma sintered samples. The data shows that an increase in milling hours is associated with a higher rate of grain growth in smaller particle size samples. This effect results from the elevated surface and grain boundary area in higher-hour milled powders, promoting particle agglomeration and rapid grain growth during SPS.

Coercive Field (Hc): In multi-domain ferromagnetic particles, Hc is significantly influenced by grain size and particle size. Typically, Hc decreases as grain size decreases, reaching its maximum value when nanoparticles transition into single domain particles.

Impact of Coercive Field with varying % of Fe-Ni: The coercive field values for the initial Fe and Ni powders were determined to be 24 Oe and 22 Oe, respectively, using VSM. Intriguingly, a two-hour milled sample exhibits a substantial increase in Hc compared to the initial values of iron and nickel (24 and 22 Oe). Specifically, Hc values are measured at 47 Oe for 40% Ni-Fe, 64 Oe for 50% Ni-Fe, and 85 Oe for 75% Ni-Fe. Moustafa<sup>17</sup> attributes this increase in Hc to the weak particle-toparticle interaction between iron and nickel. However, for samples with higher nickel content, the experimental results reveal a reduction in Hc within the range of 8 to 64 hours of milling. The Hc values for 8, 16, 32, and 64 hours of ball milling for 40-75% Ni-Fe are 32, 17, 29, 17, 35, 22 Oe, and 41, 23 Oe, respectively. These results indicate lower coercive fields for higher nickel content alloys, consistent with Marsh's 18 findings in 1938 and Qin's 19 observations in 1999.

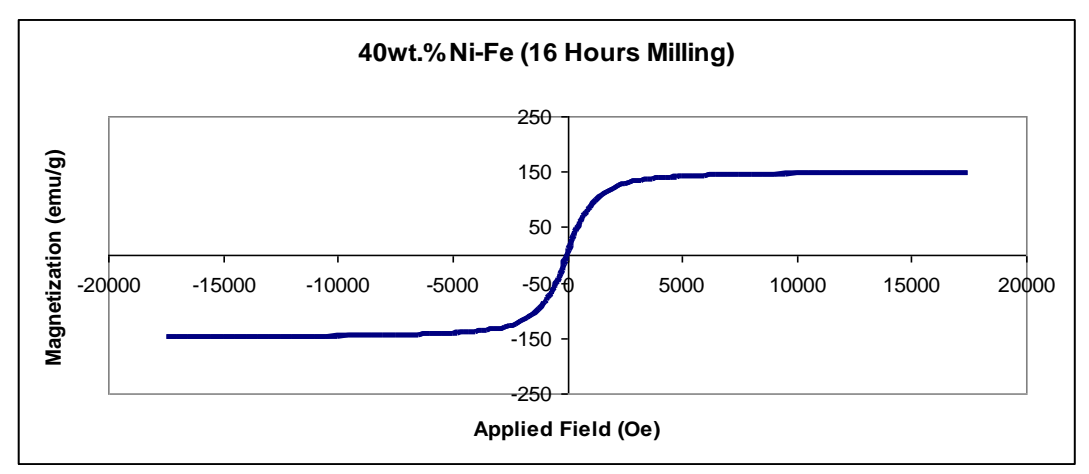


**Figure-4:** Magnetic Behavior of 40wt. % Ni-Fe Powder Sample.

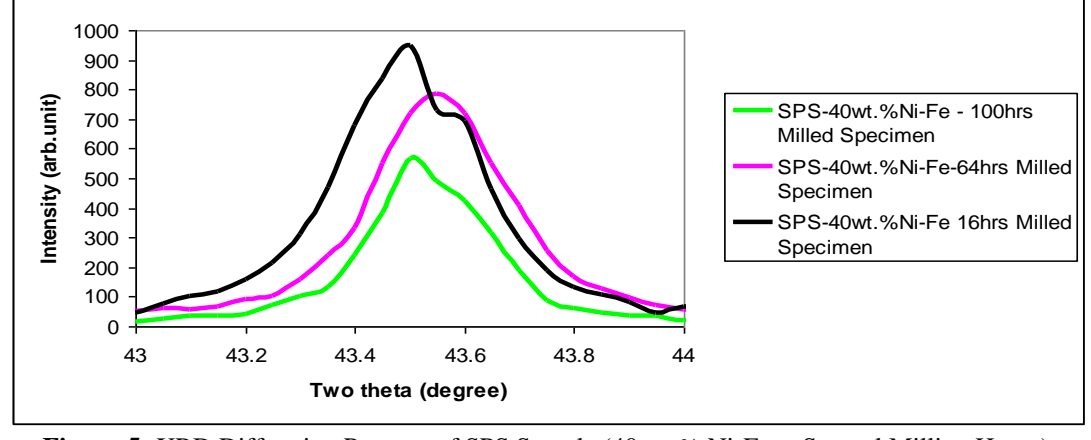


Figure-5: XRD Diffraction Patterns of SPS Sample (40wt. % Ni-Fe at Several Milling Hours).

Impact of Changes in Grain Size on Coercive Field: Figure-7 illustrates the impact of grain size on the variation in Hc. It's clear that as grain size decreases, Hc increases. For instance, in a 40% Ni-Fe alloy, Hc reaches its maximum value of 47 Oe when the grain size is 110 nm, decreasing to 29 Oe when the grain size is 73 nm, and eventually increasing to 45 Oe with a grain size of 7 nm. Similar trends are observed for 50% and 75% Ni-Fe alloys. In general, the changes in Hc values decrease within the grain size range of 250 to 75 nm. Smaller grain size samples exhibit higher lattice imperfections and internal strain, contributing to a decrease in Hc.

Impact of Changes in Particle Size on Coercive Field: The effects of particle size on Hc are shown in Figure-8. Notably, higher Hc values are observed in larger particle size samples,

and Hc decreases as particle size reduces during milling. A decrease in Hc values is noted until a critical particle size is reached, beyond which Hc values remain nearly constant until a second critical dimension is reached. Further reductions in particle size result in increased Hc. These observations are consistent with the strong particle-particle interactions that occur when particle size decreases to a certain level.

**Impact of Spark Plasma Sintering on Coercive Field:** Figure-9 demonstrates the impact of Spark Plasma Sintering (SPS) on Hc values. SPS samples generally exhibit increased Hc values as milling hours rise, indicating a correlation between Hc and grain size, imperfection lattice, and internal strain in higher-hour milled samples. This aligns with findings by Chicinas<sup>20</sup>.

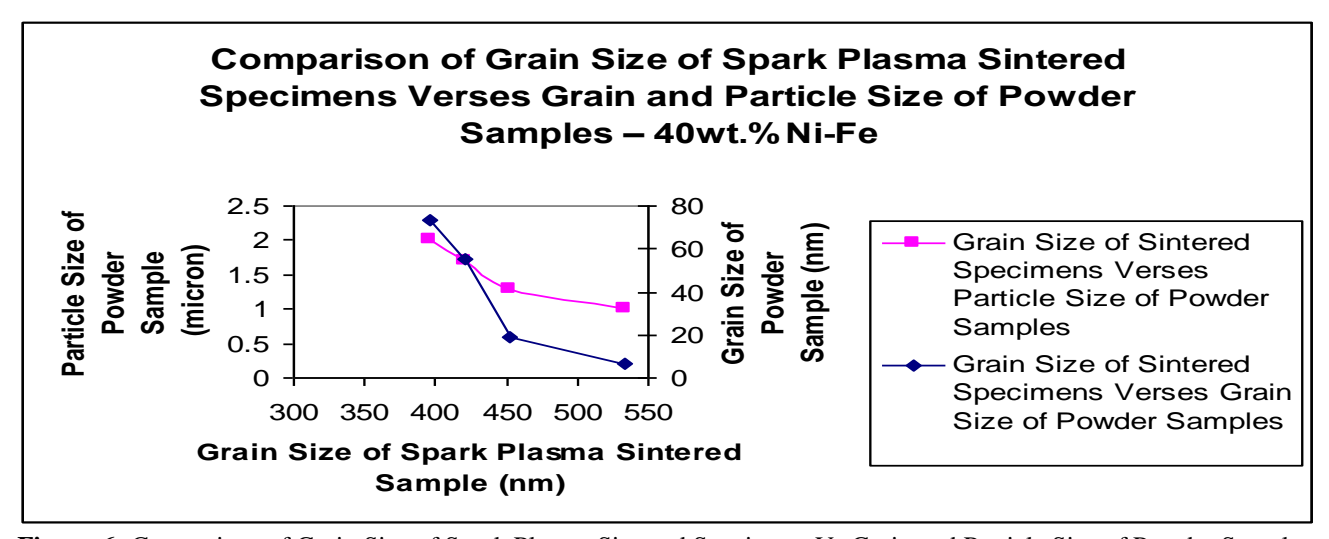


Figure-6: Comparison of Grain Size of Spark Plasma Sintered Specimens Vs Grain and Particle Size of Powder Samples.

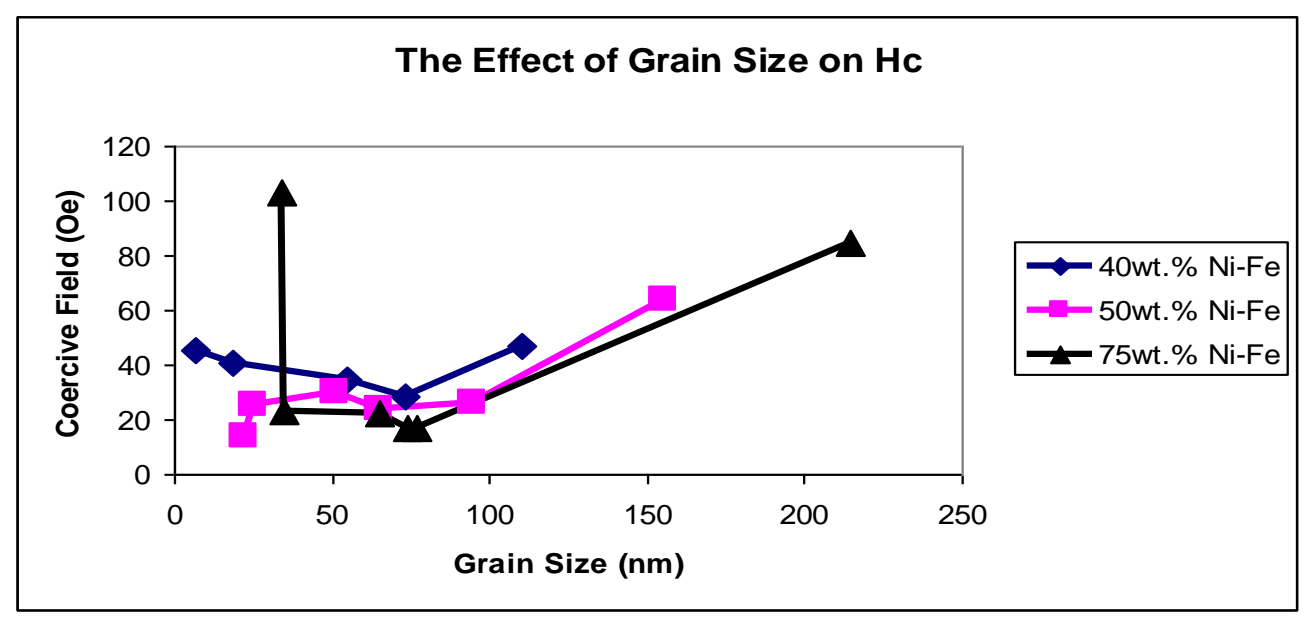


Figure-7: The Impact of Grain Size on Coercive Field.

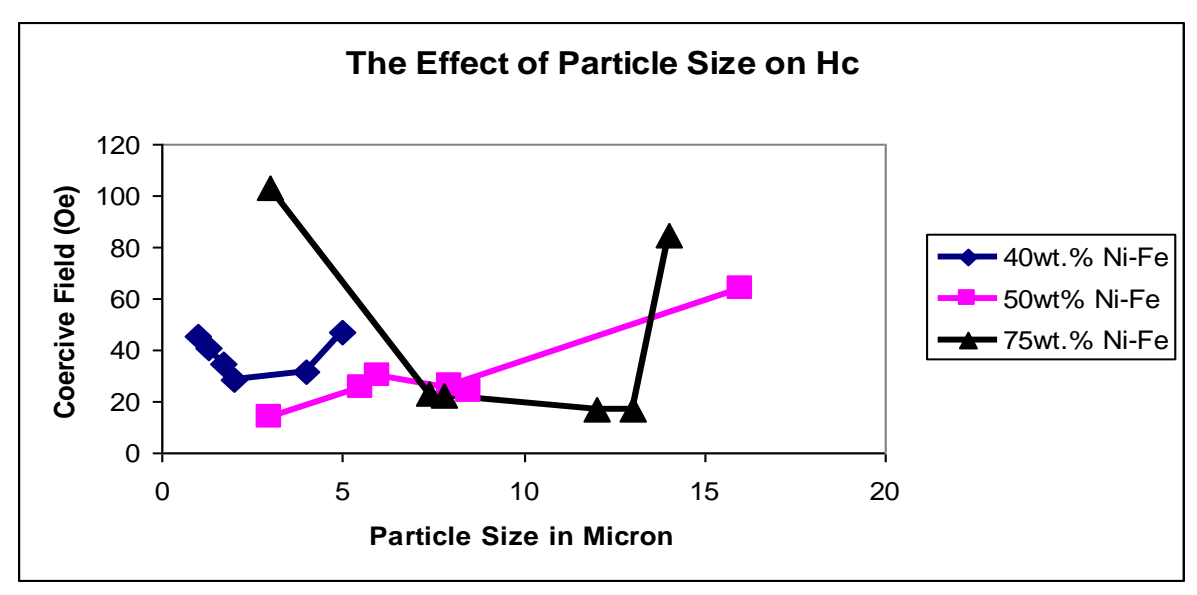
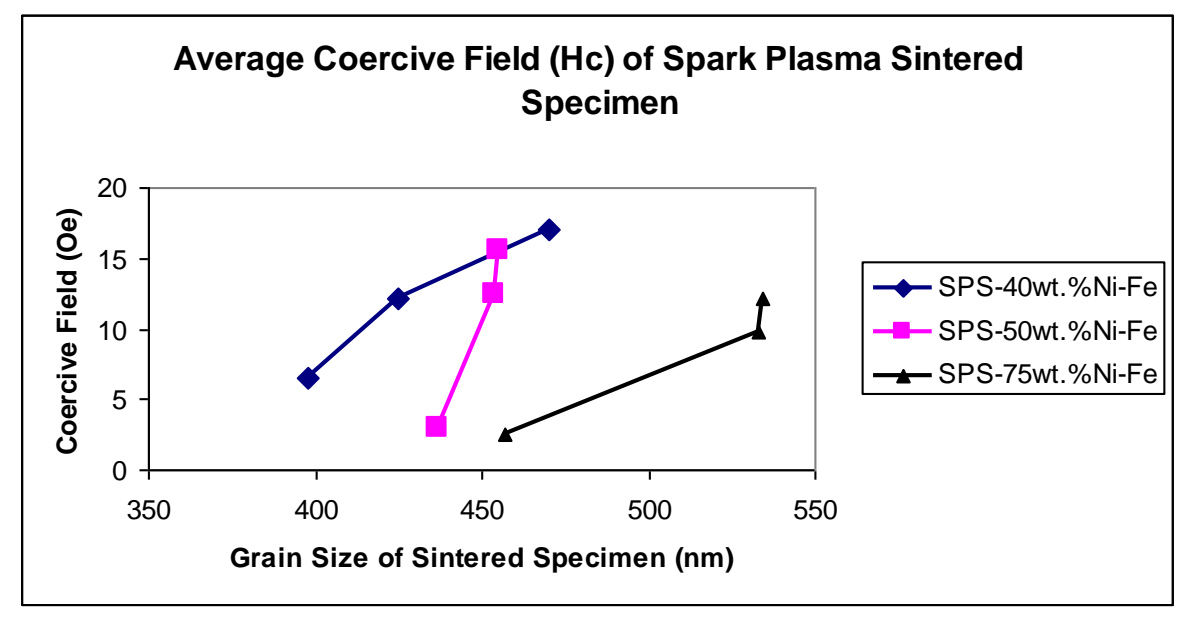


Figure-8: The Impact of Particle Size on Coercive Field.



**Figure-9:** The Impact of SPS on Coercive Field.

# Conclusion

In summary, the following key findings emerge from this study: Coercive Field and Grain Size: The coercive field (Hc) values exhibit a noticeable reduction with decreasing grain size in the range of 250 to 75 nm. Notably, a particularly high Hc value of 103 Oe is observed in the 75 wt. % Ni-Fe alloy after a 100-hour milling process. This exceptional Hc value serves as a strong indicator of the formation of single domain grains in this specific sample.

Coercive Field and Particle Size: A decrease in Hc values is evident until a critical particle size is reached. Subsequently, Hc

values remain nearly constant until a second critical dimension is achieved. Beyond this point, further reductions in particle size lead to an increase in Hc. This observed behavior underlines the intricate relationship between particle size and coercivity.

Spark Plasma Sintering (SPS) Impact: It is noteworthy that the coercive field values of all SPS samples are consistently lower than those of the powder samples. This effect indicates that the sintering process influences the magnetic properties of the material, with reduced coercivity in the sintered specimens.

These findings collectively emphasize the intricate interplay between grain size, particle size, and the sintering process in determining the coercive field of Fe-Ni alloys. Understanding these relationships is crucial for tailoring the magnetic properties of such materials for specific applications. Further research in this area promises valuable insights into the optimization of magnetic materials for various technological and industrial uses.

## References

- 1. You C, Wang S, Zhang J, Yang N and Na. Tian (2016). Improvement of magnetic hysteresis loss, corrosion resistance, and compressive strength through spark plasma sintering magnetocaloric LaFe11.65Si1.35/Cu core-shell powders. *AIP Adv.*, 6, 055321.
- 2. Shamba P, Morley N A, Cespedes O, Reaney I M, and Rainforth W M (2016). Optimization of magnetocaloric properties of arc-melted and spark plasma-sintered LaFe11.6Si1.4. *Appl. Phys. A*, 122, 732.
- 3. Qazi, U.Y., Yuan, C.Z., Ullah, N., Jiang, Y.F., Imran, M., Zeb, A., Zhao, S.J., Javaid, R., Xu, A.W. (2017). One-Step Growth of Iron-Nickel Bimetallic Nanoparticles on FeNi Alloy Foils: Highly Efficient Advanced Electrodes for the Oxygen Evolution Reaction. *ACS Appl. Mater. Interfaces*, 9, 28627-28634.
- **4.** Polychronis, G., Al Jabbari, Y. S., Eliades, T., & Zinelis, S. (2018). Galvanic coupling of steel and gold alloy lingual brackets with orthodontic wires: Is corrosion a concern?. *The Angle Orthodontist*, 88(4), 450-457.
- Barakat, N. A., El-Deen, A. G., Ghouri, Z. K., & Al-Meer, S. (2018). Stable N-doped & FeNi-decorated graphene nonprecious electro catalyst for Oxygen Reduction Reaction in Acid Medium. *Scientific REpORtS*, 8(1), 3757.
- **6.** Jang, H. C., Ju, S. H., & Kang, Y. C. (2010). Characteristics of fine size Fe-Ni alloy powders directly prepared by spray pyrolysis. *Metals and Materials International*, 16(4), 643-647.
- 7. Farahbakhsh, I., & Farahbakhsh, A. (2015). Mechanical Synthesis of Iron and Nickel Solid Solution by High Energy Ball Milling for Packaging. *J. Appl. Environ. Biol. Sci.*, 4(11S), 203-208.
- **8.** Du, S. W., & Ramanujan, R. V. (2005). Mechanical alloying of Fe–Ni based nanostructured magnetic materials. *Journal of magnetism and magnetic materials*, 292, 286-298.
- **9.** Bui, T. T., Le, X. Q., To, D. P., & Nguyen, V. T. (2013). Investigation of typical properties of nanocrystalline iron

- powders prepared by ball milling techniques. *Advances in Natural Sciences: Nanoscience and Nanotechnology*, 4(4), 045003.
- **10.** Ashokkumar, T., Rajadurai, A., & Gopinath, S. C. (2018). Saturation magnetization studies on iron-nickel ball milling nanopowders and spark plasma sintered specimens. *Journal of Magnetism and Magnetic Materials*, 465, 621-625.
- **11.** Ashokkumar, T., Rajadurai, A., & Gopinath, S. C. (2019). A study of magnetic retardation of iron-nickel nanopowder and sintered specimen by spark plasma. *Journal of Magnetism and Magnetic Materials*, 485, 280-285.
- **12.** Yelsukov, E. P., Lomayeva, S. F., Konygin, G. N., Dorofeev, G. A., Povstugar, V. I., Mikhailova, S. S., ... & Kadikova, A. H. (1999). Structure, phase composition and magnetic characteristics of the nanocrystalline iron obtained by mechanical milling in heptane. *Nanostructured Materials*, 12(1-4), 483-486.
- **13.** Sedláček, V., & Freundlich, J. (1986). Non-ferrous metals and alloys.
- **14.** Ashokkumar, T., Rajadurai, A., Gouthama, & Hussami, L. L. (2013). A study of densification and on factors affecting the density of Ni x–Fe100– x nanopowders prepared by mechanical alloying and sintered by spark plasma. *The International Journal of Advanced Manufacturing Technology*, 65(9), 1201-1213.
- **15.** Tronc, E., Jolivet, J., Dormann, J., & Fiorani, D. (1992). Magnetic Properties of Fine Particles.
- **16.** Robert, F. (2004). Paleomagnetism: Magnetic domains to geologic terranes. *Electronic Edition, Portland Univ*.
- **17.** Moustafa, S. F., & Daoush, W. M. (2007). Synthesis of nano-sized Fe–Ni powder by chemical process for magnetic applications. *Journal of materials processing technology*, 181(1-3), 59-63.
- **18.** Marsh, J. S. (1938). *The Alloys of Iron and Nickel*. Vol. 11. *Engineering foundation*.
- **19.** Qin, X. Y., Kim, J. G., & Lee, J. S. (1999). Synthesis and magnetic properties of nanostructure *γ*-Ni-Fe alloys. *Nanostructured materials*, 11(2), 259-270.
- 20. Chicinaş, I., Pop, V., Isnard, O., Le Breton, J. M., & Juraszek, J. (2003). Synthesis and magnetic properties of Ni3Fe intermetallic compound obtained by mechanical alloying. *Journal of alloys and compounds*, 352(1-2), 34-40.